Supplementary Data

Supplementary Methods

Human samples and preparation

PBMCs were separated by density gradient centrifugation with Ficoll-Paque Plus (1744003; Cytiva, Marlborough, MA, US). The cells were washed twice with phosphate-buffered saline (PBS) and resuspended in TC-Protector (KBTCP001; KAC, Kyoto, Japan), and stored in liquid nitrogen for further analysis.

Mice and cell lines

Pathogen-free C57BL/6 (B6) mice (aged 6 – 8 weeks) were obtained from Charles River, Japan. All mice were maintained under specific pathogen-free conditions and this study was approved by the Institutional Animal Care and Use Committee and carried out according to RIKEN guidelines. The K562 and HEK293 cell lines were purchased from the American Type Culture Collection (Manassas, VA, US). HEK293 cells expressing high levels of CD1d ($CD1d^{hi}$-HEK293) were generated through retroviral transduction, as previously described (1). All cells were cultured in RPMI1640 (30264-56, Nacalai Tesque, Kyoto, Japan) supplemented with 10% fetal calf serum, HEPS (30264-56, Nacalai Tesque, Kyoto, Japan), 2-mercaptoethanol (21985-023, Gibco, Waltham, MA, US), and penicillin-streptomycin (15070-063, Gibco).

Establishment of mDC/Gal

Murine DCs were generated from bone marrow progenitors in the presence of GM-CSF. On day 6, 100 ng/ml α-GalCer was added to DCs for 40 h, and 100 ng/ml LPS was added for the last 16 h to mature the DCs**.**

Flow cytometry

Frequencies and mean fluorescence intensities (MFI) of PBMCs were obtained by flow cytometric analysis with following antibodies: anti-Vα24 (C15, Beckman Coulter, Brea, CA, US), CD3 (HIT3a, BioLegend, San Diego, CA, US), CD45RA (HI100, BioLegend; all labeled with FITC), Vβ11 (C21, Beckman Coulter), CD56 (B159, BioLegend), Foxp3 (236A/E71, BioLegend; all labeled with PE); CD4 (RPA-T4, BioLegend; labeled with PerCP-Cy5.5),

NKG2D (1D11, BioLegend), DNAM-1 (118A, BioLegend), PD-1 (EH12.2H7, BioLegend), Mouse IgG1 (MOPC-21, BioLegend; all labeled with PE-Cy7), CD3 (HIT3a, BioLegend; labeled with APC), and CD19 (HIB19, BioLegend), CD16 (3G8, BioLegend), and CD8α (RPA-T8, BioLegend; all labeled with Pacific Blue); and Live/Dead Fixable Aqua (L34956, Invitrogen, Waltham, MA, USA). The detailed specifications and concentrations of the antibodies used are shown in **Supplementary Table S3**. Cells were incubated with Human TruStain FcX (422302, BioLegend) in FACS buffer (PBS with 2% heat-inactivated FBS) for Fc-blockade and then stained with surface antibodies. For Foxp3 intracellular staining, cells were fixed and permeabilized with the Foxp3/Transcription Factor Staining Buffer Set (00-5523-00, eBiosceince, San Diego, CA, US) according to the supplier's manual. All cells were analyzed using a FACSCanto II instrument with a BD FACSDiva (BD Biosciences, Franklin Lakes, NJ, US), and obtained data were analyzed using FlowJo software (Tree Star, Ashland, OR, USA). $CD4^+Foxp3^+$ T cells were further subdivided according to CD45RA expression as previously described (2).

$V\alpha24^+$ NKT expansion assay and intracellular cytokine staining

For assessing the effects of $V\alpha24^+$ NKT-cell stimulation, PBMCs (1×10^5 cells) in 200 μL of R10 were co-cultured with mDC/Gal (1×10^4 cells) and 100 U/mL of rIL-2 (Imunace, Shionogi & Co.,Ltd., Osaka, Japan) in a 96-well round-bottomed plate for 7 days. For IFN-γ intracellular staining, expanded $V\alpha24^+$ NKT cells were pre-cultured with or without mDC/Gal for 6 h in the presence of GolgiPlug (555029, BD Biosciences). Subsequently, the cells were incubated with Human TruStain FcX in FACS buffer for Fc-Blockade and then stained with surface antibodies, anti-TCR Vα24-Jα18-PE (6B11, BioLegend) and -CD3-FITC, and Live/Dead Fixable Aqua for 30 min. For intracellular cytokine staining, the cells were washed twice with FACS buffer, fixed and permeabilized using BD Cytofix/Cytoperm solution (554722, BD Biosciences) and then intracellularly stained with anti-IFN-γ-APC (B27, BioLegend) for further 30 min.

Cytotoxicity assay

After stimulation with $CD1d^{hi}$-HEK293 cells loaded with α-GalCer (CD1d/Gal) for 7 days, cytotoxicity against the cell lines (K562) was assessed. Cytotoxic activities were analyzed using the LDH Cytotoxicity Detection Kit (MK401, Takara Bio Inc., Shiga, Japan) according to the

manufacturer's instructions. Briefly, 1×10^4 target cells were co-cultured with various effector:target (E:T) ratios (1:1, 3:1, or 10:1) for 6 h. The culture supernatant was incubated with a freshly prepared reaction mixture containing tetrazolium salt, and the absorbance was measured at 490 nm. Data reported are mean ± SD of triplicate wells from three independent experiments. After the background control value was subtracted, cytotoxicity values (%) were calculated as Cytotoxiciy (%) = [(effector:target cell mix - effector cell control) - spontaneous target cell control] / (maximum target control - spontaneous target cell control) × 100.

TCGA-CESC data acquisition

Open access RNA-seq data from TCGA cervical squamous cell carcinoma and endocervical adenocarcinoma (TCGA-CESC) cohort were gathered from TCGA Data Portal (https://portal.gdc.cancer.gov/) in September 2022 (n = 304). Clinical data were collected from each patient. Gene expression levels were categorized into two groups based on median values of transcripts per million.

Preprocessing of single cell RNA sequencing (scRNA-seq)

We utilized two human CC patient datasets from Gene expression Omnibus (Accession number: GSE168652 and GSE208653) (3,4). These datasets contained the barcode.tsv, feature.tsv and matrix.mtx data of tumor patients and healthy participants. We created a Seurat object and integrated it with Read.10X (10X genomics).

Integration of scRNA-seq datasets and clustering

These datasets were transformed to a Seurat Object using CreateSeuratObject function in RStudio, and then merged into one object. We computed UMAP embeddings and clustering using Harmony algorithms. The relative cell populations of these clusters were determined based on the representative gene signatures as T cells (*CD3E*), NK cells (*GNLY*), B cells (*MS4A1*), mast cells (*TPSB2*), plasma cells (*JCHAIN*), myeloid (*ITGAM*), macrophage (*CD68*), DC (*ITGAX*), neutrophil (*CSF3R*), basal epitherial (*KRT19* and *EPCAM*), germ cell (*CENPF*), endothelial cell (*AGP1*), fibroblast (*DCN*), and smooth muscle endothelial (*C11orf96*). The expression of *CD3E*, *NCAM1*, and *FCGR3A* was assessed in the clusters consisting of T cells and NK cells. They were classified as T cells (*CD3E*) and NK cells (*NCAM1* and *FCGR3A)*

based on the expression levels of these genes. The T-cell population was assessed for *CD4*, *CD8*, and *CD40LG* expression and was further classified into CTL cells (*CD8*) or Th cells (*CD4* and *CD40LG*). We further computed the UMAP embeddings and clustering of the CTL cells cluster and calculated CTL gene signatures (3) (*Gzmk*, *KLRB1*, *XCL1*, *CAPG*, *Havcr2*, *Pdcd1*, *Glny*, *Cd160*, *Kir2dl4*, *Klrc2*, *Ifit1*, *Ifit44L*, and *TCF7*). The cell population of CTL clusters was determined based on the expression of gene signatures including those for IFN-stimulated T-cell (*IFIT1*, *IFIT44L*), IEL-like T-cell (*CD160*, *KIR2DL4*, *KLRC2*), exhausted T-cell (*HAVCR2*, *PDCD1*), progenitor exhausted T-cell (*HAVCR2*, *PDCD1*, *TCF7*), resident memory T-cell (*XCL1*, *IGTAE*) recently activated effector memory T-cell (*CXCR1*,*FCGR3A*,*FGFBP2*), MAIT-like T-cell (*KLRB1*) and effector memory T-cell (*GZMK*).

Supplementary Table S1 Characteristics of patients with CC

	Age	FIGO Stage	Histology	Cancer Recurrence	Treatment	Analysis (PBMC)	Analysis (multiplex IHC)
CC01	62	IB1	Adeno-carcinoma	-	OP+CT	✓	✓
CC02	50	IB1	SCC	-	OP+CT	✓	
CC03	58	IIIC1r	SCC	-	CCRT	✓	✓
CC04	88	IIB	SCC	-	RT	✓	
CC05	44	IIIC1r	SCC	-	CCRT	✓	✓
CC06	57	IIIB	Adeno-carcinoma	+	CCRT	✓	
CC07	38	IIIC1r	Neuro-endocrine	+	NAC+OP	✓	
CC08	49	IIIC1r	SCC	-	CCRT	✓	
CC09	47	IB3	SCC	+	OP+CT	✓	✓
CC10	61	IIIC1r	SCC	+	CCRT	✓	
CC11	63	IB2	SCC	-	OP	✓	✓
CC12	77	IVB	SCC	-	CCRT	✓	✓
CC13	73	IIB	SCC	-	CCRT	✓	
CC14	34	IB2	SCC	-	OP+RT		✓
CC15	74	IIIC1r	SCC	-	OP+CCRT		✓
CC16	55	IB2	SCC	-	OP+CCRT		✓
CC17	30	IB1	SCC	-	OP+CCRT		✓
CC18	58	IIB	SCC	-	OP+CCRT		✓
CC19	70	IIA	SCC	-	OP		✓
CC20	42	IB	SCC	-	OP+RT		✓
CC21	40	IB2	SCC	+	OP+CCRT		✓
CC22	62	IIIC	SCC	+	OP		✓
CC23	47	IIA2	SCC	+	OP		✓

Abbreviations: SCC, squamous cell carcinoma; OP, surgical operation; CT, chemotherapy; RT, radiation therapy; CCRT, concurrent chemoradiotherapy; NAC, neo-adjuvant chemotherapy

Supplementary Table S2 Panels for multiplex IHC

	Primary Ab				Secondary Ab		Detection	
	Antigen	Clone	Manufacturer	Concentration	Target	Concentration	Fluorescent	Concentration
Panel 1:	Foxp3	D2W8E	Cell Signaling Technologies	1/100	Anti-Rb IgG	1/500	Opal 570	1/200
Lymphocyte	CD4	EP204	Diagnostic BioSystems	1/200	Anti-Rb IgG	1/500	Opal 650	1/200
Panel	CD3ε	CAL54	Abcam	1/1000	Anti-Rb IgG	1/500	Opal 520	1/200
	CD56	EP2567Y	Abcam	1/2000	Anti-Rb IgG	1/500	Opal 690	1/200
	PD-1	NAT105	Abcam	1/50	Anti-Mo IgG	1/1000	Opal 540	1/200
	pan CK	AE1/AE3	Abcam	1/20 (ab27988) or 1/100 (ab80826)	Anti-Mo IgG	1/1000	Opal 620	1/200
	DAPI			1/4000				
Panel 2:	LAG-3	EPR20261	Abcam	1/1000	Anti-Rb IgG	1/500	Opal 570	1/200
T-cell	CD8α	CAL66	Abcam	1/1940	Anti-Rb IgG	1/500	Opal 650	1/200
Markers	CD3ε	CAL54	Abcam	1/1000	Anti-Rb IgG	1/500	Opal 520	1/200
Panel	TIM-3	D5D5R	Cell Signaling Technologies	1/400	Anti-Rb IgG	1/500	Opal 690	1/200
	OX40	Ber-Act35	BioLegend	1/50	Anti-Mo IgG	1/1000	Opal 540	1/200
	pan CK	AE1/AE3	Abcam	1/20 (ab27988) or 1/100 (ab80826)	Anti-Mo IgG	1/1000	Opal 620	1/200
	DAPI			1/4000				
Panel 3:	CD69		Abcam	1/500	Anti-Rb IgG	1/500	Opal 570	1/200
Resident	CD8α	CAL66	Abcam	1/1940	Anti-Rb IgG	1/500	Opal 650	1/200
Memory	CD103		Abcam	1/1000	Anti-Rb IgG	1/500	Opal 520	1/200
T-cell Panel	pan CK	AE1/AE3	Abcam	1/20 (ab27988)	Anti-Mo IgG	1/1000	Opal 620	1/200
	DAPI			1/4000				
Panel 4:	CD3ε	CAL54	Abcam	1/1000	Anti-Rb IgG	1/500	Opal 520	1/200
NKG2D Panel	CD56	EP2567Y	Abcam	1/2000	Anti-Rb IgG	1/500	Opal 690	1/200
	CD8α	CAL66	Abcam	1/1940	Anti-Rb IgG	1/500	Opal 650	1/200
	pan CK	AE1/AE3	Abcam	1/20 (ab27988) or 1/100 (ab80826)	Anti-Mo IgG	1/1000	Opal 620	1/200
	NKG2D	1D11	Abcam	1/100	Anti-biotin	1/250	Opal 570	1/200
	DAPI			1/4000				

Supplementary Table S3 Panels for flow cytometry

Marker	Clone	Fluorophore	Manufacturer	Identifier	Concentration
CD3	HIT3a	APC	Biolegend	300312	1/400
CD19	HIB19	Pacific Blue	Biolegend	302224	1/50
V α 24	C15	FITC	Beckman	IM1589	1/25
V β 11	C21	PE	Beckman	IM2290	1/25
CD4	RPA-T4	PerCP-Cy5.5	Biolegend	300530	1/100
CD3	HIT3a	FITC	Biolegend	300306	1/200
CD56 (NCAM)	B159	PE	Biolegend	318306	1/200
CD16	3G8	Pacific Blue	Biolegend	302032	1/1200
CD314 (NKG2D)	1D11	PE-Cy7	Biolegend	320812	1/200
CD226 (DNAM-1)	118A	PE-Cy7	Biolegend	338316	1/200
Mouse IgG1, k	MOPC-21	PE-Cy7	Biolegend	400126	1/200
CD3	HIT3a	APC	Biolegend	300312	1/400
CD8a	RPA-T8	Pacific Blue	Biolegend	301023	1/200
CD4	RPA-T4	PerCP-Cy5.5	Biolegend	300530	1/100
CD45RA	HI100	FITC	Biolegend	304106	1/200
Foxp3	236A/E71	PE	Biolegend	400126	1/20
CD279 (PD-1)	EH12.2H7	PE-Cy7	Biolegend	329917	1/200
Mouse IgG1, k	MOPC-21	PE-Cy7	Biolegend	400126	1/200
CD3	HIT3a	FITC	Biolegend	300306	1/20
CD4	RPA-T4	PerCP-Cy5.5	Biolegend	300530	1/100
CD8	SK1	BUV737	BD Horizon	612754	1/500
CD134 (OX40)	Ber-ACT35	Alexa647	Biolegend	350018	1/20
Mouse IgG1, k	MOPC-21	Alexa647	Biolegend	400130	1/25

CD223 (LAG-3)	**11C3C65**	**BV711**	**Biolegend**	**369320**	**1/20**
Mouse IgG1, k	**MOPC-21**	**BV711**	**Biolegend**	**400168**	**1/100**
TIM-3	**F38-2E2**	**PE**	**Biolegend**	**345006**	**1/100**
Mouse IgG1, k	**MOPC-21**	**PE**	**Biolegend**	**555749**	**1/200**
CD279 (PD-1)	**EH12.2H7**	**PE-Cy7**	**Biolegend**	**329917**	**1/200**
Mouse IgG1, k	**MOPC-21**	**PE-Cy7**	**Biolegend**	**400126**	**1/10000**

Supplementary Figure S1

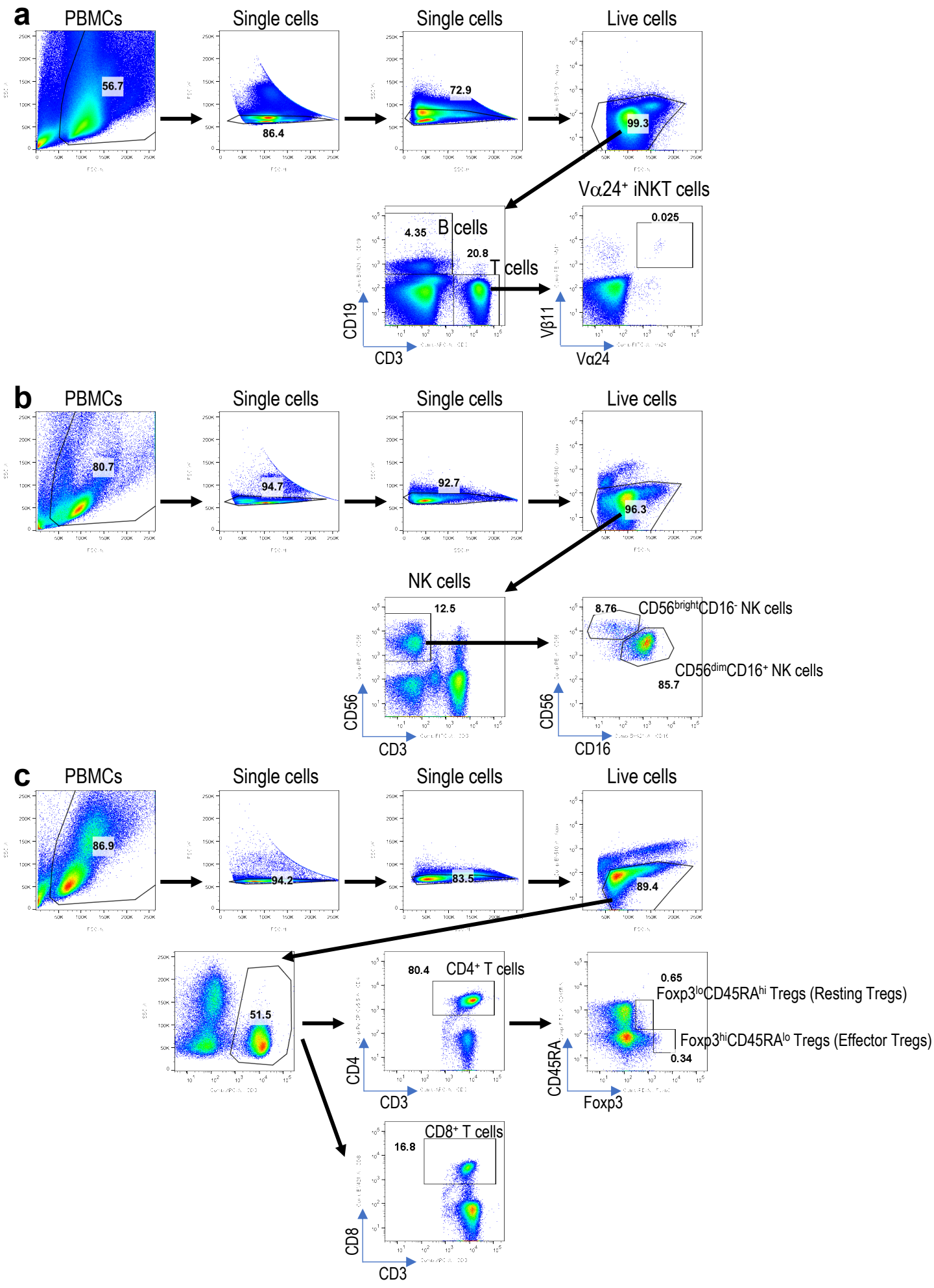

Supplementary Figure S2

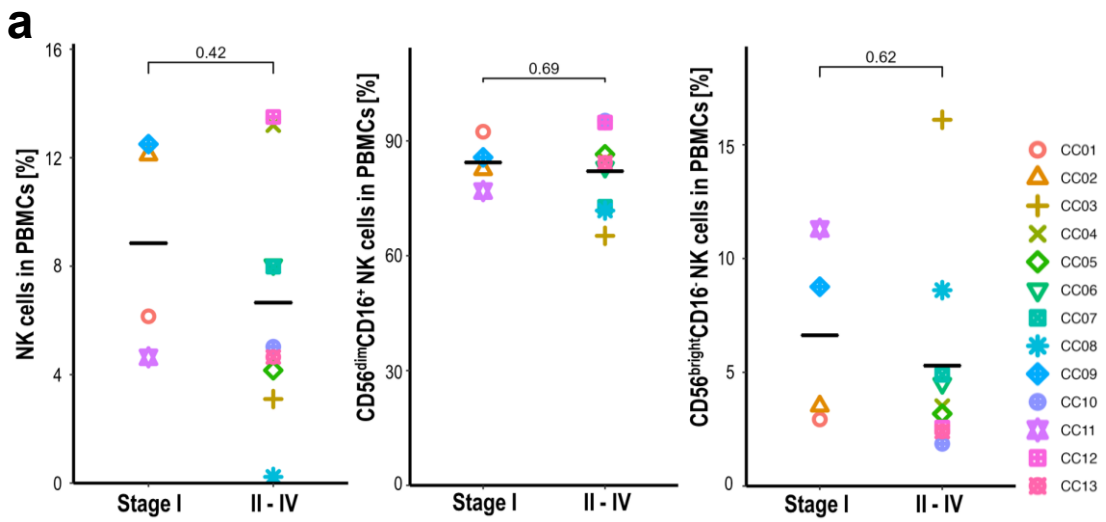

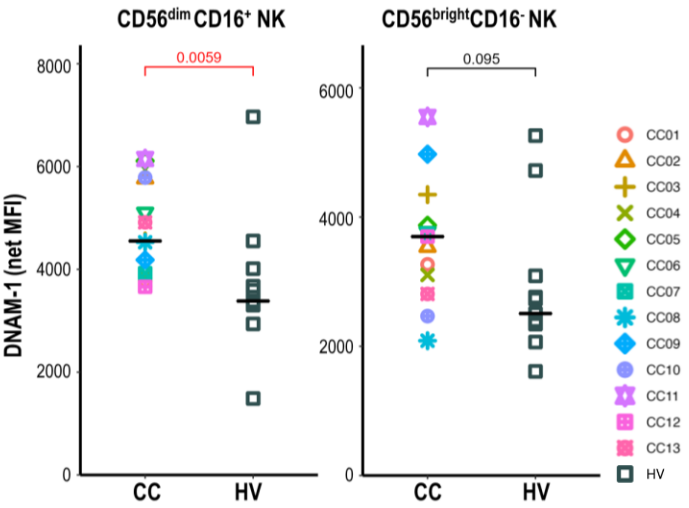

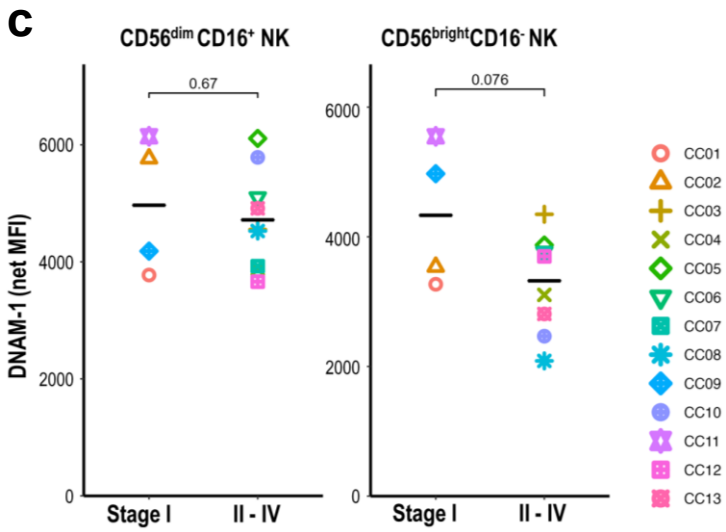

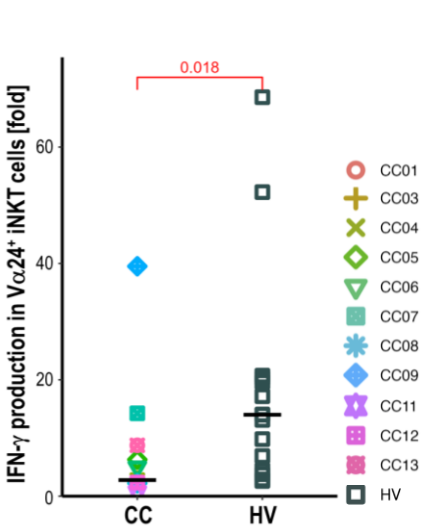

Supplementary Figure S3

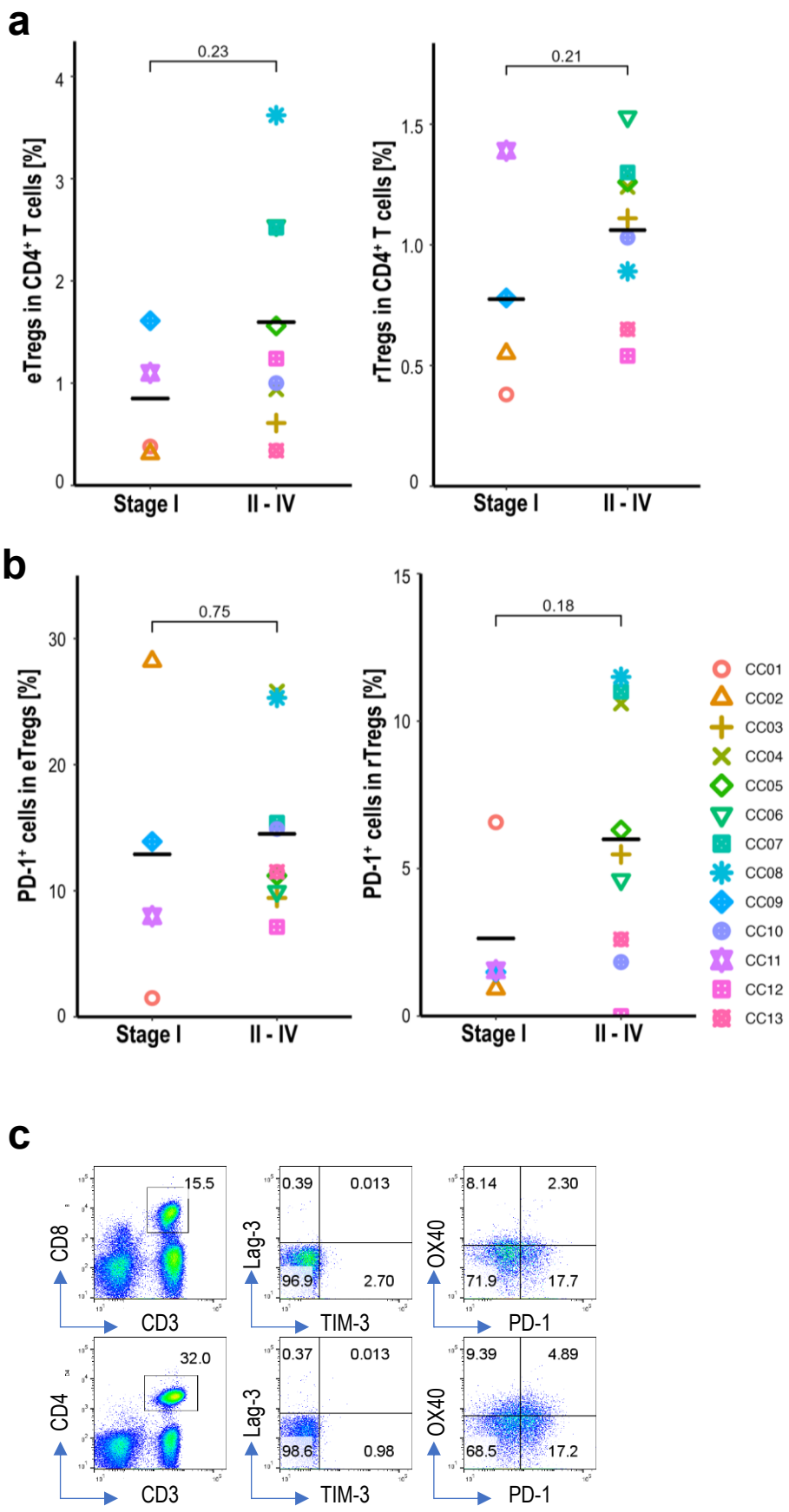

Supplementary Figure S4

a

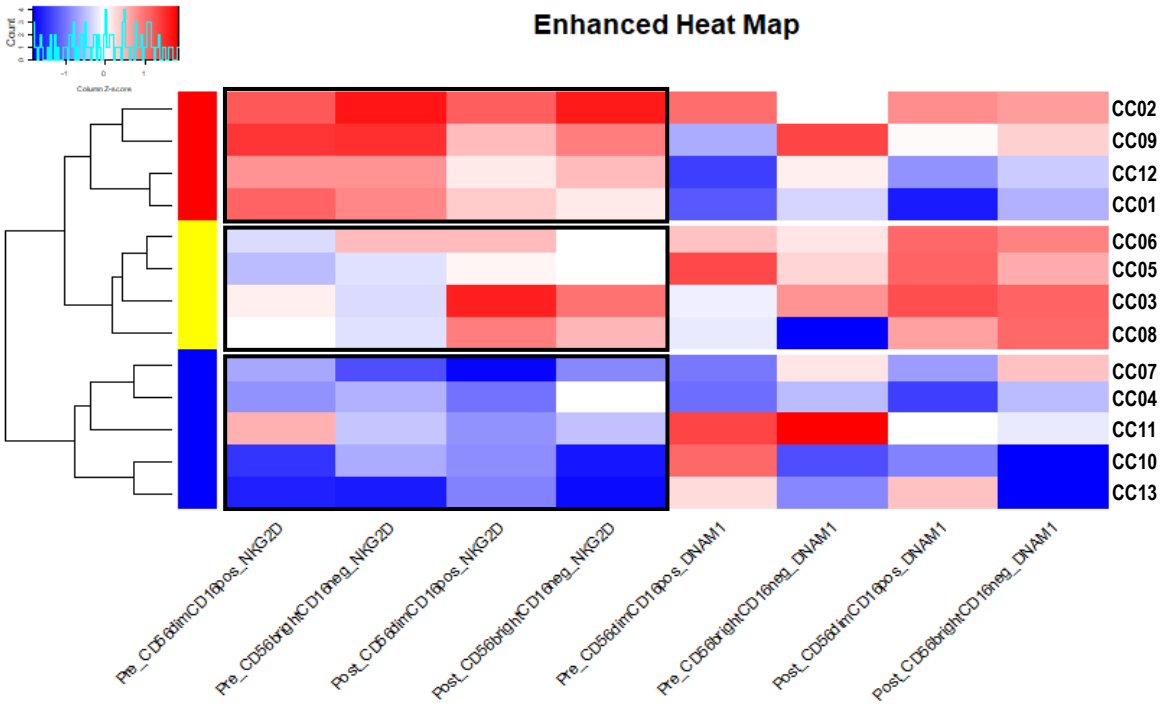

b

KLRK1 **(NKG2D)**

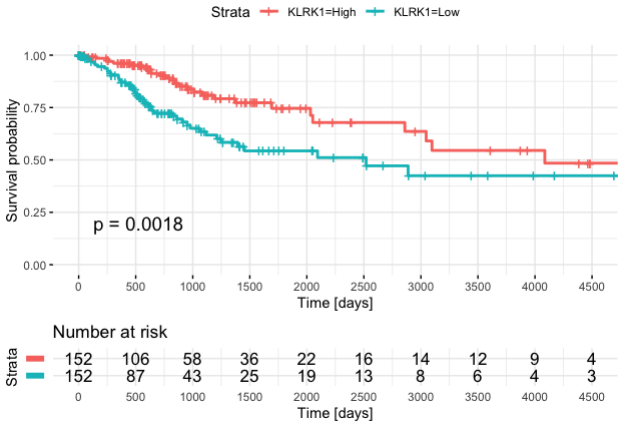

c

CD226 **(DNAM-1)**

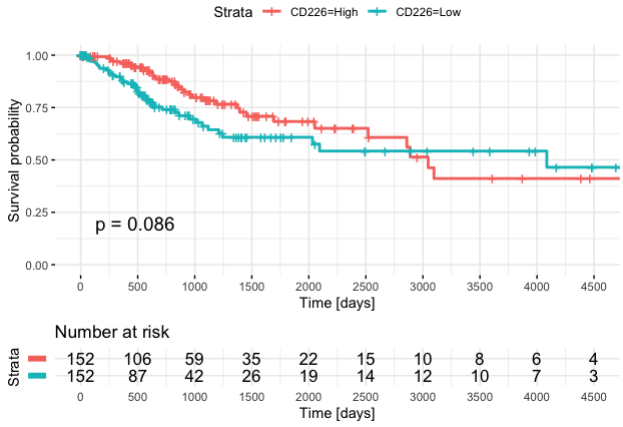

Supplementary Figure S5

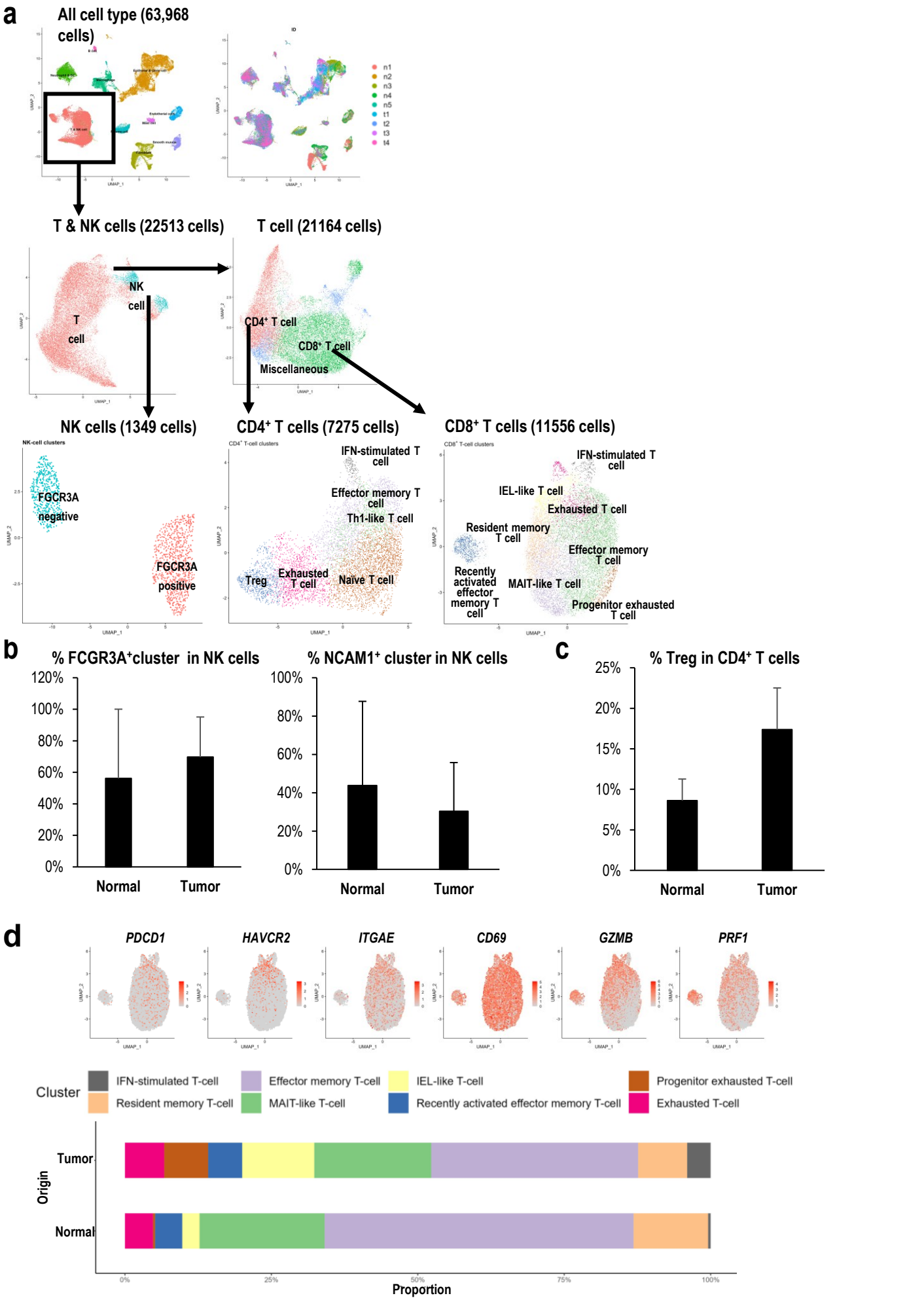

Supplementary Figure S6

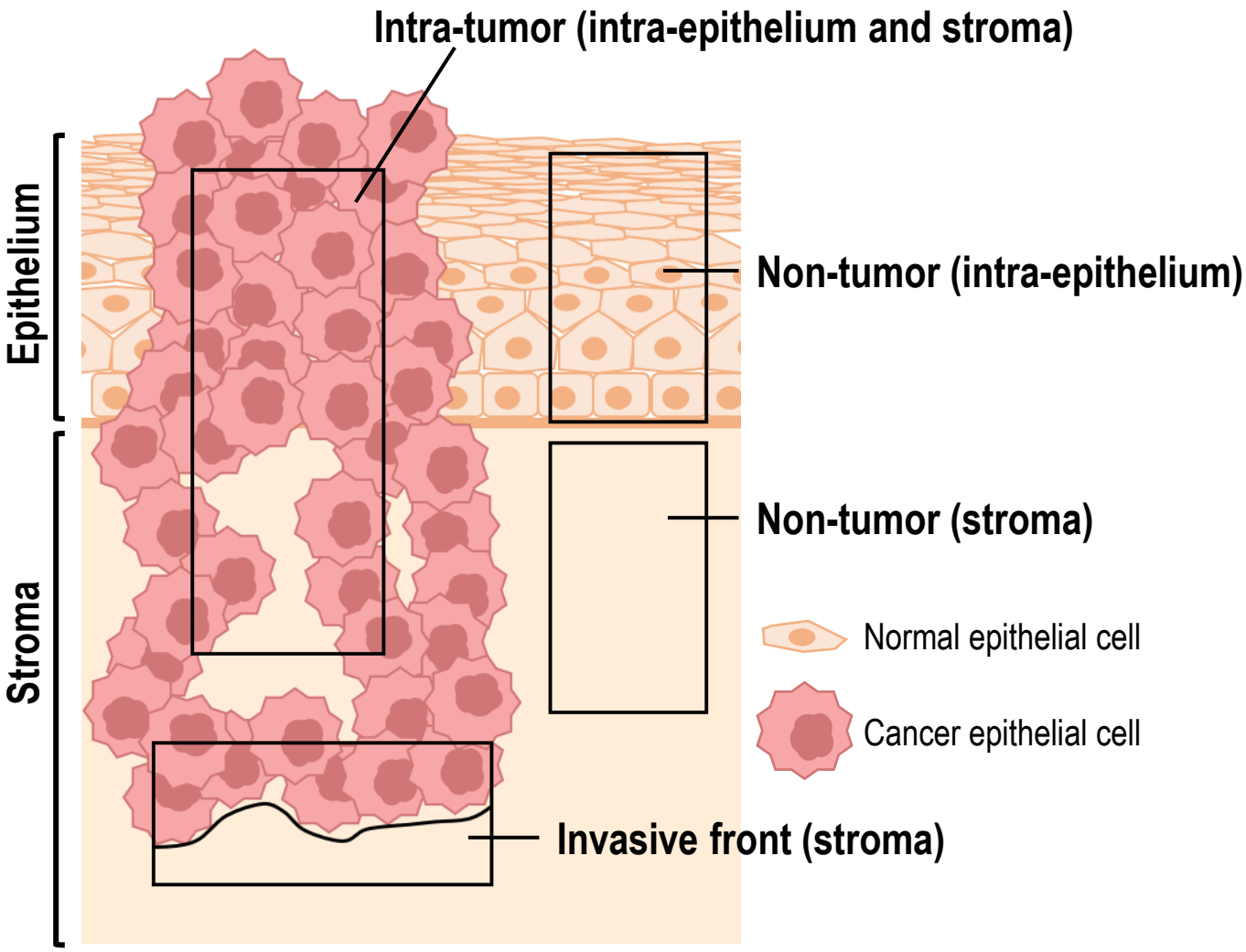

Supplementary Figure S7

a

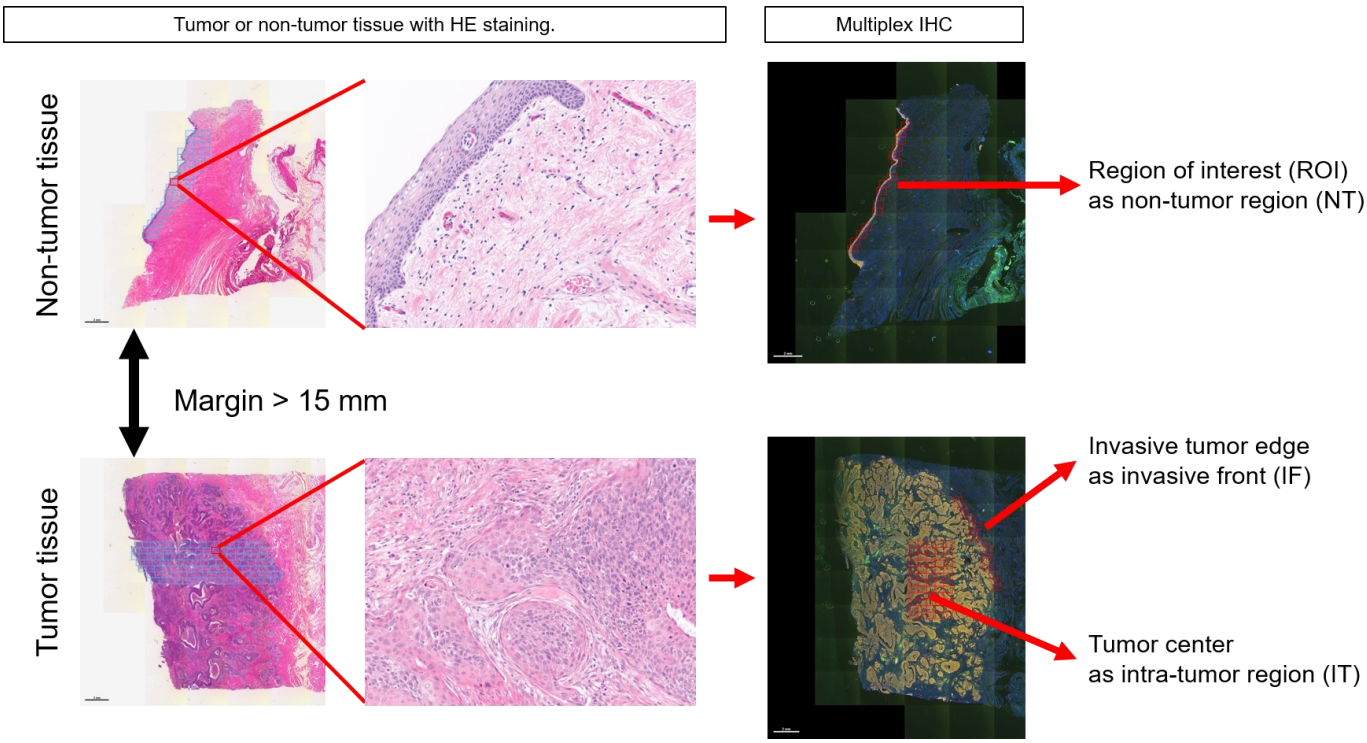

b

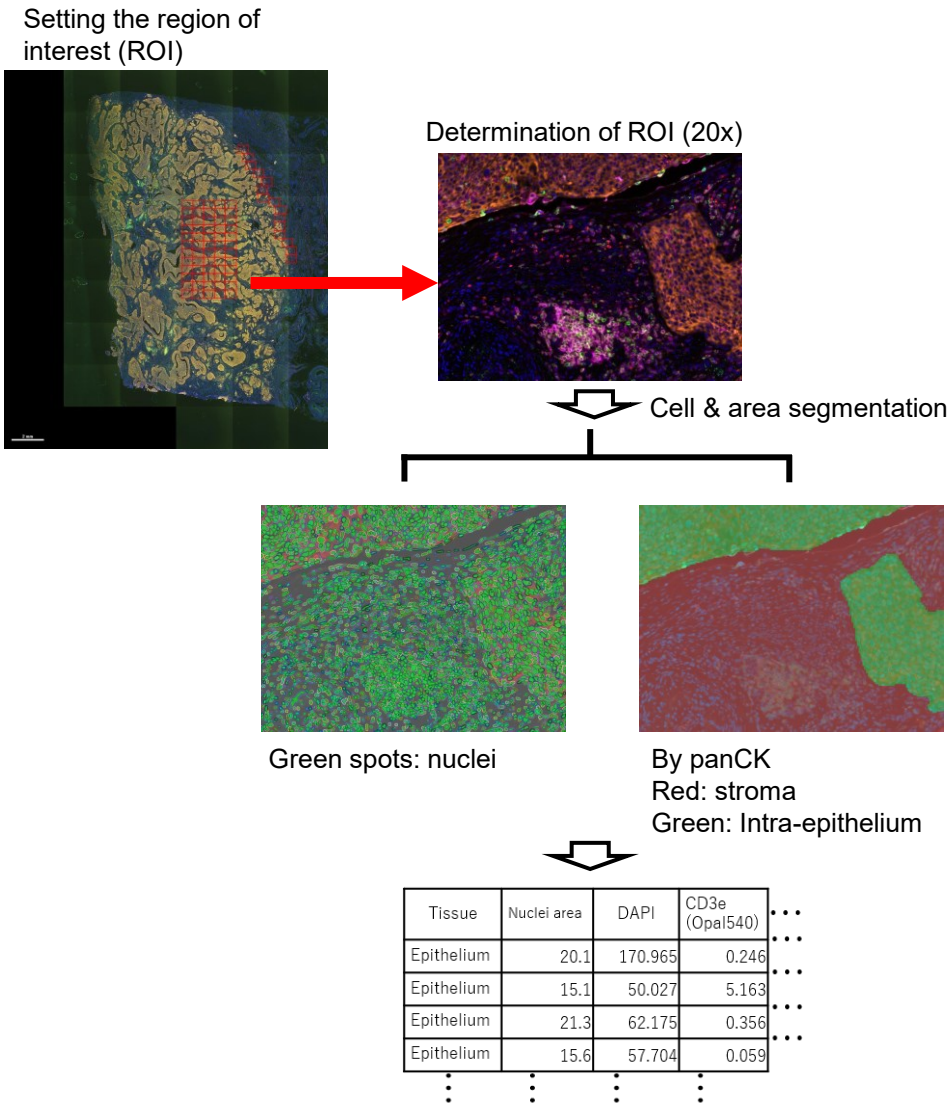

Tissue	Nuclei area	DAPI	CD3e (Opal540)	...
Epithelium	20.1	170.965	0.246	...
Epithelium	15.1	50.027	5.163	...
Epithelium	21.3	62.175	0.356	...
Epithelium	15.6	57.704	0.059	...
⋮	⋮	⋮	⋮	

Supplementary Figure Legends

Supplementary Figure S1. Flow cytometry gating strategy for PBMCs

(**a**) Gating strategy for assessing the frequency of Vα24^{+} iNKT cells. Vα24^{+} NKT cells were assessed using Vα24-FITC and Vβ11-PE after gating CD3-APC. (**b**) Gating strategy for assessing NK cells subsets to classify CD56^{bright} CD16^{-} or CD56^{dim} CD16^{+} NK cells using CD56-PE and CD16-Pacific Blue after gating CD3-FITC. (**c**) Gating strategy for assessing T cells. T cell subset was assessed using CD4-PerCP/Cy5.5 and CD8-Pacific Blue after gating CD3-APC. CD4^{+}T cells were further divided using CD45RA-FITC and Foxp3-PE to classify eTregs and rTregs.

Supplementary Figure S2. NK cell analysis in patients with CC

(**a**) The frequency and subset of NK cells in PBMCs among patients with CC Stage I versus II-IV were compared (stage I [*n* = 4] and stage II-IV [*n* = 9] patients). (**b**) The expression of DNAM-1 in NK subsets among patients with CC versus HV was compared. (**c**) The expression of DNAM-1 in NK subsets among patients with CC Stage I versus II-IV was compared. (**d**) Fold change of IFN-γ production in Vα24^{+} iNKT cells of pre- and post-stimulation with 1×10^{5} mDC/Gal among patients with CC versus HV was compared. Student's t-test was used in (**a**) and Wilcoxon rank sum test was used in (**b**)-(**d**) to assess the statistical significance. Each symbol represents an individual sample, the horizontal bars indicate means of the groups in (**a**), and the median MFI in (**b**)-(**d**). The numbers showed *p*-value.

Supplementary Figure S3. Comparison of the frequency of CD4^{+} eTreg cells and PD-1^{+} CD4^{+} eTreg cells among patient with CC stages

The frequency of eTreg in CD4^{+} T cells (**a**) or the frequency of PD-1^{+} CD4^{+} T cells in CD4^{+} eTreg cells (**b**) among patients with CC Stage I versus II-IV was compared (stage I [*n* = 4] and stage II-IV [*n* = 9] patients). Student's t-test was used to assess the statistical significance. Each symbol represents an individual sample, the horizontal bars indicate means of the groups. The numbers showed *p*-value. (**c**) Phenotype of CD8^{+} or CD4^{+} T cells. Expression of LAG-3, TIM-3, PD-1 and OX40 on CD8^{+} or CD4^{+} T cells was analyzed using CD223 (LAG-3)-BV711, TIM-3-

PE, CD279 (PD-1)-PE-Cy7, and CD134 (OX40)-Alexa647 after gating CD3-FITC in combination with CD4-PerCP-Cy5.5 and CD8-BUV737. Representative flow cytometry data are shown.

Supplementary Figure S4. Expression of NKG2D and DNAM-1 in NK cells and exhaustion markers in CD8$^+$T cells in patients with CC

(**a**) Features of patients with patients with CC were clustered into three groups using hierarchical clustering method. The Z-score was obtained after normalization with the Box-Cox transformation. The Euclidean distance and Ward's method were used to build a dendrogram. (**b, c**) The effects of activating (**b**) and inhibitory (**c**) NK receptor expression in the overall survival of patients with CC were assessed using bulk RNA-seq data obtained from the TCGA open access database (n = 304). These data were collected in September 2022 from the TCGA portal (https://portal.gdc.cancer.gov/). In our assay, TPM was used for normalized read count and the R package "*survival*" was used for survival analysis. The groups over the median value were defined as "High" and those below were defined as "Low". The survival curves were plotted using the Kaplan-Meier method, and p-values were calculated with the log-rank test. The high expression of *KLRK1* significantly improved overall survival of patients with CC.

Supplementary Figure S5. scRNA-seq analysis of normal and tumor tissues of patients with CC

A Seurat object was generated from two human CC patient datasets from Gene expression Omnibus (Accession number: GSE168652 and GSE208653)(5, 6). The relative cell populations of these clusters were determined based on the representative gene signatures as shown in materials and methods in detail. (**a**) Overview of the core CC atlas and NK, CD4$^+$ and CD8$^+$ T cell components. (**b**) The proportions of NK clusters (FCCR3A and NCAM1) in normal and tumor tissues. (**c**) The proportion of Treg cluster in CD4$^+$ T cells in normal and tumor tissues. (**d**) UMAP plot showing all CD8$^+$ T cells. *PDCD1, HAVCR2, ITGAE, CD69, GZMB, and PRF1e*xpression in CD8$^+$ T cells, as shown in UMAP plots. Proportions of each CD8$^+$ T cluster in normal and tumor tissues.

Supplementary Figure S6. Classification of Intra-tumor (IT), Invasion Front (IF), and Non-tumor (NT) Areas

Intra-tumor (IT) is distributed from the epithelium to the stroma, encompassing both regions within the tumor mass. The edge of the tumor region, where the tumor cells are actively invading the surrounding stroma, is referred to as the invasion front (IF). The non-tumor (NT) region includes the epithelial tissue and stroma located outside the tumor region, serving as a reference for normal tissue architecture.

Supplementary Figure S7. Histological confirmation and multiplex immunohistochemistry analysis of tumor and non-tumor tissue samples

(**a**) Samples were obtained from non-tumor (NT) and tumor tissues and histologically confirmed with hematoxylin-eosin (HE) staining. NT was selected from cervical or vaginal tissue without cancer cells at least 15 mm distant from the tumor tissue, and ROIs were selected from the NT region. ROIs for the intra-tumor (IT) and invasive front (IF) were selected from the tumor center or edge by referencing within HE and panCK staining. (**b**) Fluorescence images were acquired from each region of interest (ROI) after staining the samples with multiplex immunohistochemistry (mIHC) (20x magnification). Cell segmentation was performed with the inForm image analysis software (PerkinElmer) based on nuclei (green) (left), followed by area segmentation (stroma [red] and intra-epithelium [green]) using pan cytokeratin (panCK) staining. Subsequently, fluorescent intensity and area information were obtained from data gathered using batch analysis provided by the inForm software. Fluorescent intensity data were analyzed with FloJo to obtain the immune cell subsets and cell counts. After calculating the fluorescent intensity, cell frequency was determined as the number of cells divided by stromal or epithelial area (cells/mm^2 stroma or epithelium (bottom).

Supplementary References

1. Shimizu K, Mizuno T, Shinga J, Asakura M, Kakimi K, Ishii Y*, et al.* Vaccination with antigen-transfected, NKT cell ligand-loaded, human cells elicits robust in situ immune responses by dendritic cells. *Cancer Res* 2013;**73**(1):62-73 doi 10.1158/0008-5472.CAN-12-0759. 0008-5472.CAN-12-0759 [pii].
2. Miyara M, Yoshioka Y, Kitoh A, Shima T, Wing K, Niwa A*, et al.* Functional delineation and differentiation dynamics of human CD4+ T cells expressing the FoxP3 transcription factor. *Immunity* 2009;**30**(6):899-911 doi 10.1016/j.immuni.2009.03.019.
3. Guo C, Qu X, Tang X, Song Y, Wang J, Hua K*, et al.* Spatiotemporally deciphering the mysterious mechanism of persistent HPV-induced malignant transition and immune remodelling from HPV-infected normal cervix, precancer to cervical cancer: Integrating single-cell RNA-sequencing and spatial transcriptome. *Clin Transl Med* 2023;**13**(3):e1219 doi 10.1002/ctm2.1219.
4. Li C, Guo L, Li S, Hua K. Single-cell transcriptomics reveals the landscape of intra-tumoral heterogeneity and transcriptional activities of ECs in CC. *Mol Ther Nucleic Acids* 2021;**24**:682-94 doi 10.1016/j.omtn.2021.03.017.
5. Guo, C., Qu, X., Tang, X., Song, Y., Wang, J., Hua, K. et al. Spatiotemporally deciphering the mysterious mechanism of persistent HPV-induced malignant transition and immune remodelling from HPV-infected normal cervix, precancer to cervical cancer: Integrating single-cell RNA-sequencing and spatial transcriptome. Clin Transl Med 13, e1219 (2023).
6. Li, C., Guo, L., Li, S. & Hua, K. Single-cell transcriptomics reveals the landscape of intra-tumoral heterogeneity and transcriptional activities of ECs in CC. Mol Ther Nucleic Acids 24, 682-694 (2021).